Phobos, The Early Years*

George S.F. Stephans

Massachusetts Institute of Technology

For the Phobos Collaboration
B.B.Back[1], M.D.Baker[2], D.S.Barton[2], R.R.Betts[1,6], R.Bindel[7], A.Budzanowski[3], W.Busza[4], A.Carroll[2], M.P.Decowski[4], E.Garcia[6], N.George[1], K.Gulbrandsen[4], S.Gushue[2], C.Halliwell[6], G.A.Heintzelman[2], C.Henderson[4], D.J.Hofman[6], R.Hołyński[3], B.Holzman[2,6], E.Johnson[8], J.L.Kane[4], J.Katzy[4,6], N.Khan[8], W.Kucewicz[6], P.Kulinich[4], W.T.Lin[5], S.Manly[8], D.McLeod[6], J.Michałowski[3], A.C.Mignerey[7], J.Mülmenstädt[4], R.Nouicer[6], A.Olszewski[2,3], R.Pak[2], I.C.Park[8], H.Pernegger[4], C.Reed[4], L.P.Remsberg[2], M.Reuter[6], C.Roland[4], G.Roland[4], L.Rosenberg[4], P.Sarin[4], P.Sawicki[3], W.Skulski[8], S.G.Steadman[4], P.Steinberg[2], G.S.F.Stephans[4], M.Stodulski[3], A.Sukhanov[2], J.-L.Tang[5], R.Teng[8], A.Trzupek[3], C.Vale[4], G.J.van Nieuwenhuizen[4], R.Verdier[4], B.Wadsworth[4], F.L.H.Wolfs[8], B.Wosiek[3], K.Woźniak[3], A.H.Wuosmaa[1], B.Wysłouch[4]

[1] Argonne National Laboratory, Argonne, IL 60439, USA
[2] Brookhaven National Laboratory, Upton, NY 11973, USA
[3] Institute of Nuclear Physics, Kraków, Poland
[4] Massachusetts Institute of Technology, Cambridge, MA 02139, USA
[5] National Central University, Chung-Li, Taiwan
[6] University of Illinois at Chicago, Chicago, IL 60607, USA
[7] University of Maryland, College Park, MD 20742, USA
[8] University of Rochester, Rochester, NY 14627, USA

The Phobos detector, one of the two small detectors at RHIC, focuses on measurements of charged particle multiplicity over almost the full phase space and identified particles near mid-rapidity. Results will be presented from the early RHIC gold-gold runs at nucleon-nucleon center of mass energies of 56 and 130 GeV as well as the recently concluded run at the full RHIC energy of 200 GeV.

PACS numbers: 25.75.-q

* Presented at the Cracow Epiphany Conference on Quarks and Gluons in Extreme Conditions

1. Introduction

Phobos is one of the two small experiments included in the first round of RHIC. The two areas of physics focus are charged-particle multiplicity over all of phase space and identified particle studies near mid-rapidity. The collaboration had two primary goals. The first was to perform measurements of numerous basic observables quickly and accurately as each new beam or energy condition was provided by RHIC. This early information would determine the global characteristics of the systems being created. The initial studies would be followed by more detailed investigations exploiting the unique features of the Phobos detector which include the ability to collect a large unbiased event sample, the large segmentation and phase-space coverage for charged particle multiplicity, and the ability to extend particle measurements to low transverse momentum. In addition, the detector was designed to have relatively low mass and particle measurements starting very close to the beam pipe, resulting in high resolution and minimal backgrounds.

This talk will present a sampling of Phobos physics results on both multiplicity and identified particles. The former will include several measurements taken during the recently concluded first run of gold-gold collisions at the full RHIC energy. Ongoing analysis and future possibilities will also be discussed.

2. Experimental Details

2.1. Detector Setup

The full Phobos experimental configuration, shown in Fig. 1, was completed in early 2001. It includes trigger detectors, a multiplicity array, and a 2-arm spectrometer[1, 2, 3]. One of the unique features of the Phobos setup is the presence of a 1 mm thick Be beampipe which extends the full length of the experimental area, ± 6 m. This results is very small absorption and scattering of the primary particles as well as minimizing production of secondary particles. To further reduce these background effects, the first layers of each detector component were mounted as close as possible to the beampipe.

The primary event trigger and off-line centrality determination, were provided by two arrays of 16 scintillators ("paddle counters") located at distances of -3.21 m and 3.21 m from the nominal interaction point. These counters subtended pseudorapidities between $3 < |\eta| < 4.5$. The minimum-bias trigger for gold-gold collisions required hits in both counters within a time window consistent with an interaction near the nominal intersection point.

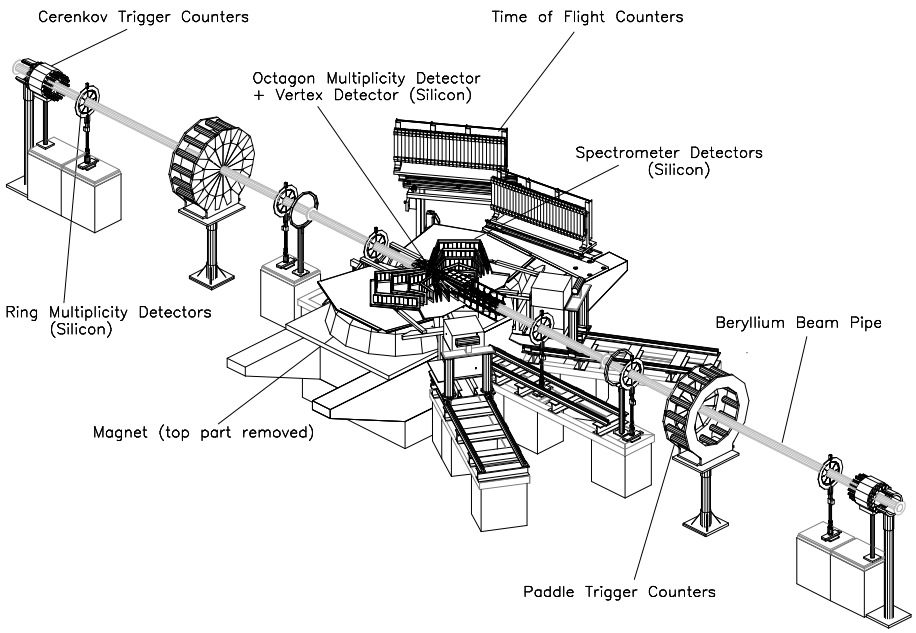

Fig. 1. Phobos detector setup for the 2001 running period.

Another important component of the event characterization concerns determining the location of the interaction along the beam pipe. For some of the data taken in the 2001 RHIC run, an online trigger on vertex location was provided by a set of special T0 counters installed in front of the Cěrenkov counters near the end of the Be beam pipe. For off-line analysis, a high precision interaction location is provided by the vertex detector consisting of two sets of two layers of Si wafers, one above and one below the beam pipe. Data from this counter also were used in extracting multiplicity information.

Two zero-degree calorimeters (ZDCP, ZDCN) at $z = \pm 18.5$ m (not shown in the figure) which are sensitive to spectator neutrons are a feature common to all four experiments at RHIC. These were used in some of the off-line analysis of the present data.

The multiplicity counter has two major components, an octagon-shaped array of Si wafers arranged parallel to the beam pipe near the interaction region, and a set of 6 ring counters (3 on each side) arranged perpendicular to the beam pipe at distances up to about 5 m away. This detector provides almost full coverage for charged particles out to a pseudo-rapidity of about 5.4 units.

The spectrometer also is constructed of Si detectors mounted in 2 symmetric horizontal arms on either side of the beam. Depending on trajectory,

particles traverse up to 16 layers of Si sensors. The two arms are located between the poles of a conventional double dipole magnet (bottom half shown in the figure). The magnet is designed to generate very little field in the first 6 planes of the spectrometer followed by a rapid rise to a roughly constant 2 T field for the remainder of the layers. The spectrometer sensors are finely segmented in the horizontal, bend-plane direction and also segmented vertically to assist in separating close tracks. These detectors provide both hit locations for tracking and also energy loss information used in particle identification. To extend the particle identification to higher momentum, one arm of the spectrometer included 2 sets of time-of-flight walls, each consisting of 120 scintillator slats (8 mm square).

2.2. Si Detector Performance

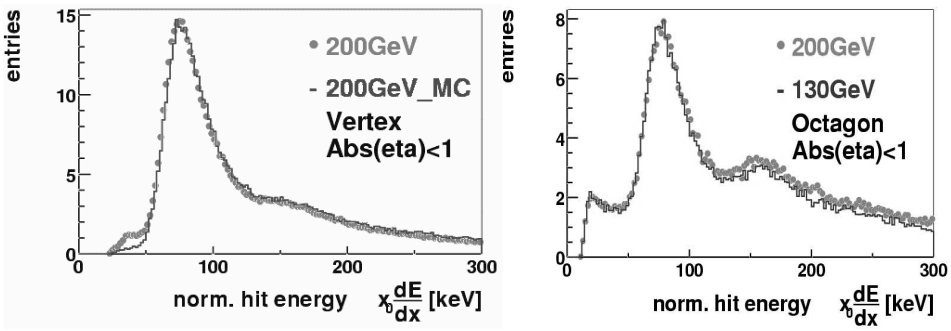

Fig. 2. Si detector performance examples. See text for discussion.

The majority of the physics measurements performed by Phobos result from data taken with the approximately 137,000 channels of Si detectors. The quality and stability of those detectors as well as the detailed understanding of their characteristics are critical to the success of the experiment. Examples of the results are shown in Fig. 2. The left panel compares the signal distribution found in the Vertex detector to the predictions of the Geant calculations. The agreement is excellent. In the time since this figure was prepared, the small discrepancy at low signal height has been corrected by improving the merging of hits due to particles that deposit energy in more than one pad. The right panel of the figure shows a comparison of the signal strength in the Octagon detector at beam energies of 130 GeV and 200 GeV taken during different running periods. The peak locations and widths were clearly very stable over this time. The slight difference in the relative height of the peaks at about 80 and 160 keV (corresponding to one and two particles traversing a single pad, respectively) is due to the roughly

15% higher multiplicity at the higher energy. The clean peaks seen in Fig. 2 demonstrate the large separation of signal and noise in the Si detectors. Average values of the ratio of signal to noise were about 18 in the spectrometer and vertex detector and about 14 in the larger pads of the octagon and ring counters. Finally, the overall quality of the detector is extremely high. The number of Si channels which do not work properly is in the range of 1-3%, where this number includes all flaws in the Si itself, the electronics, and the read-out and calibration systems.

2.3. Event Trigger and Centrality Determination

As mentioned above, the primary event trigger is generated by signals from the paddle counters[4]. Detailed studies of the data and simulations indicate that this trigger misses at most a few percent of the total gold-gold interaction rate. Also, the contributions from beam-gas collisions, beam halo, or other background sources are negligible. For off-line centrality determination, the truncated means of the calibrated ADC signals from both sets of paddles were combined to generate a distribution. Monte Carlo simulations, supported by correlations with the ZDC data, show that this signal varied monotonically with the number of participants in the interaction. Cuts were determined corresponding to set percentages of the full interaction cross-section. The results of Glauber model and Monte Carlo calculations were used to convert these percentage intervals into mean values of the number of participating nucleons for each selected region. See the talk by Andrzej Olszewski in these proceeding for more discussion of the general topic of selecting centrality.

3. Multiplicity Measurements

3.1. Advantages of the Phobos Apparatus

As described briefly above, the Phobos detector has several important characteristics which are unique at RHIC. These include almost full phase space coverage and a high granularity in both pseudo-rapidity and azimuthal angle. The beampipe, detectors, and associated mechanics were arranged to provide as little mass and as little distance as possible between the interaction point and the active elements. In addition, different detectors and several independent analysis methods for particular detectors can be used to generate multiple measurements of each observable. This wealth of results provides a powerful tool for determining and understanding the systematic uncertainties in the derived quantities. Comparison of data with very different characteristics (for example counting Si pads with hits compared to

summing the energy output of the Si) to the Monte Carlo predictions adds confidence to the quality of the final result.

3.2. Beam Energy Dependence of Mid-Rapidity Multiplicity

The first physics measurement using RHIC data was the Phobos value for the charged particle multiplicity density near mid-rapidity for gold-gold collisions at nucleon-nucleon center of mass energies of 56 and 130 GeV[5]. Recently, Phobos again produced the first physics result from the full energy RHIC run at 200 GeV[6]. A summary of the data from Phobos and the other RHIC experiments is show in Fig. 3.

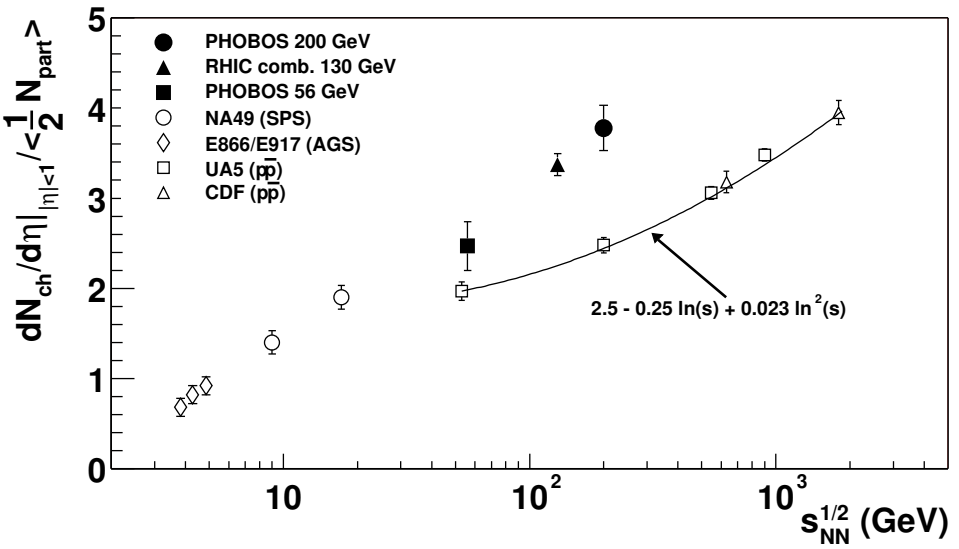

Fig. 3. Beam energy dependence of the charged particle multiplicity density per participant pair averaged over the region $|\eta| \leq 1$. Data are shown for central AuAu (AGS and RHIC) or PbPb (SPS) collisions as well as proton-antiproton collisions. See text for details and references.

The results shown are pseudo-rapidity densities of primary charged particles averaged over the region $|\eta| \leq 1$ measured in the top 6% most central events for nucleus-nucleus collisions. In order to compare to different systems (including nucleon-nucleon collisions), the densities have been divided by the number of pairs of participating nucleons. The Phobos data are shown for 56 and 200 GeV while the average of data from all 4 RHIC experiments is shown at 130 GeV[7, 8, 9]. These values are compared to those

found for lower energy nucleus-nucleus interactions [10, 11, 12] as well as proton-antiproton collisions[13]. It is clear that nucleus-nucleus collisions produce significantly more particles per interacting pair of nucleons than are produced in proton-antiproton collisions at the same energy. The data also suggest that this excess over $p\overline{p}$ may still be increasing at the highest RHIC beam energy.

Before publication of the first Phobos data, theoretical predictions for the 130 GeV number varied by more than a factor of two. The models were refined (or in some cases abandoned) resulting in later predictions of the 200 GeV multiplicity which varied by about 25%. The latest Phobos result is in significant disagreement with even some of the adjusted calculations. Thus, even this most basic of global observables has already set significant constraints on the allowable model space.

3.3. Centrality Dependence of Mid-Rapidity Multiplicity

The observed excess of normalized particle production in central ion-ion collisions, compared to nucleon-nucleon, leads naturally to the question of how this quantity depends on centrality. Fig. 4 shows Phobos data that address this question[14, 15]. As before, the quantity plotted is the primary charged particle density (averaged over ± 1 unit of pseudorapidity about midrapidity) divided by the number of participant pairs. Data are presented for a range of centralities for Au-Au collisions at 130 and 200 GeV. The statistical errors are smaller than the symbols. The shaded region around the 200 GeV points shows the range of systematic uncertainty. The range for 130 GeV is similar. The proton-antiproton points are found from data at 200 GeV and an interpolation of data to 130 GeV using the parameterization shown in Fig. 3[13]. The data suggest that the excess particle production compared to nucleon-nucleon collisions increases monotonically with possibly a steeper rise for the most peripheral and most central interactions.

The two sets of lines on Fig. 4 show the results of a gluon saturation model and an empirical parameterization in terms of a two-component model of the interactions[16, 17]. The latter separates the produced particles into two classes, the "soft" particles that scale with the number of participants and a "hard" component which scales with the number of collisions as determined from a Glauber model. The formula used is

$$\frac{dN}{d\eta} = (1-x)n_{pp}\frac{N_{part}}{2} + xn_{pp}N_{coll} \qquad (1)$$

where n_{pp} is the experimentally seen multiplicity density of particles in proton-proton or proton-antiproton collisions (about 2.2-2.4, see Fig. 3),

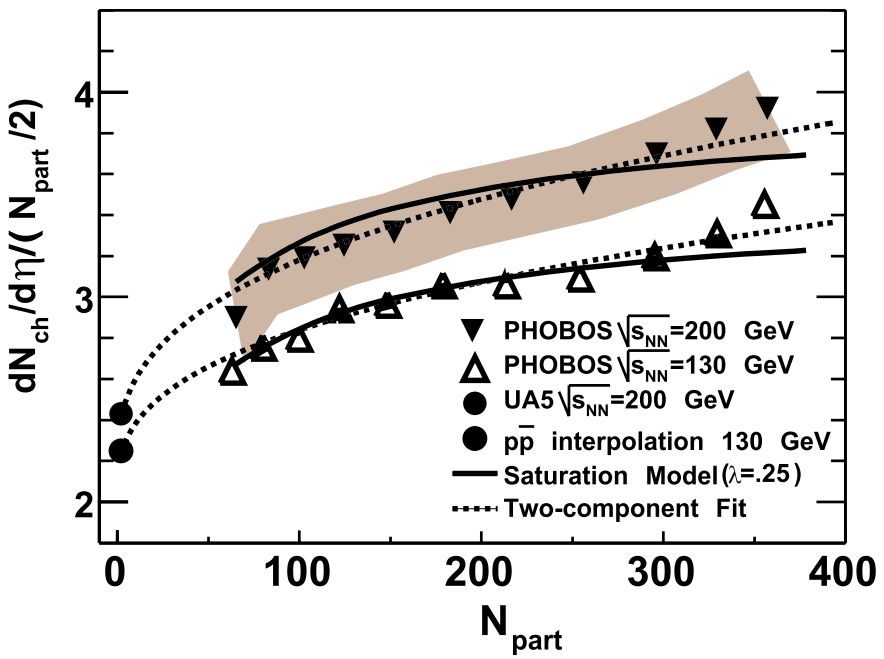

Fig. 4. Collision centrality dependence of the charged particle multiplicity density per participant pair averaged over the region $|\eta| \leq 1$. Phobos data are shown for AuAu collisions at 130 and 200 GeV energies. Statistical error bars are smaller than the symbols. The shaded region shows the systematic uncertainty at 200 GeV, the band for 130 GeV would be similar. Also shown are data from proton-antiproton collisions and the results of two theoretical calculations. See text for details and references.

N_{part} is the number of participants (2 for pp or $p\overline{p}$), and N_{coll} is the number of collisions. The only parameter not found from data or Glauber models of nucleon-nucleon collisions is x, the fraction of the particles produced by hard scattering in nucleon-nucleon collisions. For the dashed lines shown in Fig. 4, the value for x ($\approx$10%) was chosen to give a reasonable fit to the 130 GeV gold-gold data. The energy dependence of x was given by simple QCD arguments. Both models are seen to give reasonable descriptions of the experimental data. The saturation model calculation stops at a little below 100 total participants because the assumptions in the model are deemed inappropriate for more peripheral collisions.

It is interesting to recast Eq. 1 in terms of ν, the average number of collisions experienced by one of the participating nucleons. This concept has been used frequently in attempts to compare pp, pA and AA data. In

this case, we have symmetric systems so we know that $N_{pair} = \frac{N_{part}}{2}$. From nuclear geometry, the number collisions is about $N_{coll} \approx N_{pair}^{\sim 1.3-1.4}$. By definition, $N_{coll} = \nu N_{pair}$ and so $\nu \approx N_{pair}^{\sim 0.3-0.4}$. Plugging these relations into Eq. 1 yields

$$\frac{dN}{d\eta N_{pair}} = n_{pp}(1 + x(\nu - 1)) \tag{2}$$

In this model, the ratio of normalized particle density between nucleus-nucleus and nucleon-nucleon collisions is a simple mix of nuclear geometry and the fraction of hard scattering. Note that asymmetric systems (pAu, $SiAu$, etc.) will have different relationships between N_{coll} and N_{part}. Data for such systems, expected in upcoming RHIC runs, will be critical in determining the validity of these types of parameterizations.

Several conclusions can be drawn from this data and the comparison to various models. Once again, it is seen that a relatively simple "global" observable provides important constraints on the fundamental properties of the interactions. A simple model separating particle production into "soft" and "hard" components shows a reasonable extrapolation of AuAu data down to nucleon-nucleon values. Although the gluon saturation model and the two-component parameterization have very different underlying physics assumption, the predictions are very similar. Hopefully future analysis and additional data including asymmetric systems will help to differentiate between the competing models of centrality dependence. Finally, it is important to keep in mind that all the competing models involving parton dynamics agree with the conclusion that the gluon densities in the initial system are large on the QCD scale.

One intriguing observation is that the data at both beam energies appears to have an increasing slope for the most central collisions. In the context of the two component model, it is tempting to ask whether a third source of particles arises in those situations. Although it is tempting to speculate, caution must be exercised because the changes may be due to systematic uncertainties in the analysis. The two data sets are clearly statistically independent but share some aspects in the analysis which could conceivably lead to a common systematic trend.

3.4. Rapidity Distribution of Charged Particles

As mentioned previously, one unique aspect of the Phobos experiment is the ability to detect charged particles over a wide range of pseudorapidity. An example of the results for 130 GeV are shown in Fig. 5[18]. In contract to the previous plots, this figure shows total charged particle pseudorapidity density, $\frac{dN}{d\eta}$, without normalizing by the number of participants. Also, in this case the error bars include systematic uncertainties which dominate

in almost all cases. With such complete coverage, the total number of charged particles can be extracted with relatively little uncertainty due to the extrapolation into unmeasured regions. For the most central 3% of the AuAu events at 130 GeV, the total number of primary charged particles is about 4200.

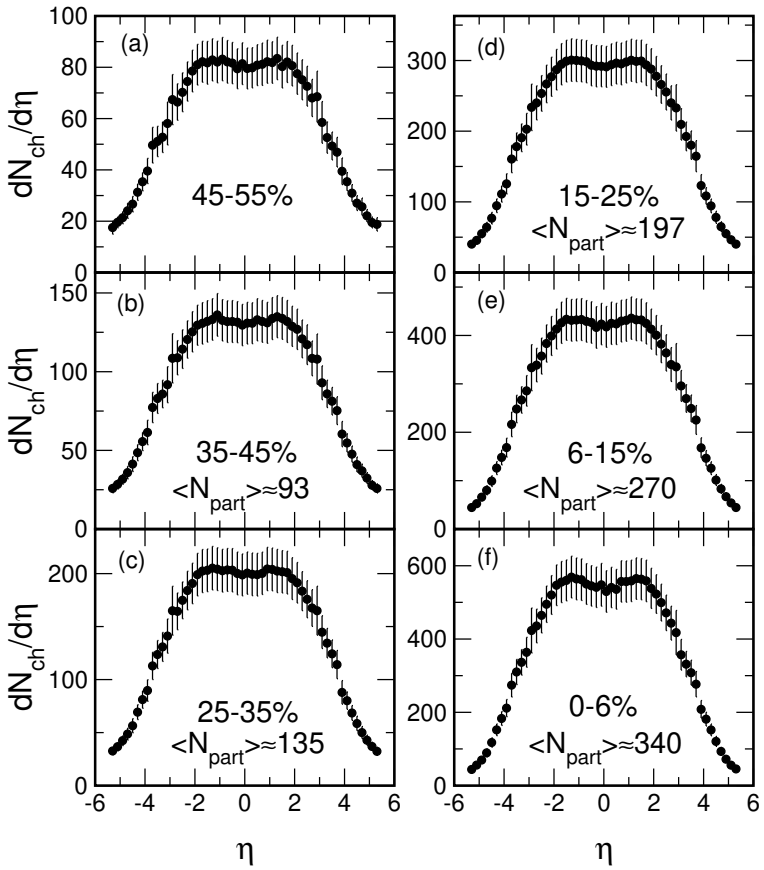

Fig. 5. Pseudorapidity dependence of the charged particle multiplicity density. Phobos data are shown for AuAu collisions at 130 GeV. The error bars include the systematic uncertainties which dominate in most cases. Distributions are shown for different centralities starting with the most peripheral at top left and the most central at bottom right. The labels show the percentage cuts on the total inelastic AuAu cross-section included in each panel as well as the average total number of participants. See text for details and references.

Each panel corresponds to a different range of centrality with the most peripheral in the upper left and the most central in the lower right. The per-

centages listed are the fraction of the total inelastic gold-gold cross-section included. The average total number of participants, found using a Glauber model, for events within the indicated centrality selection is also shown. One important feature that relates to the discussion in the preceeding section is that the distribution is relatively flat over about 2-3 units on either side of $\eta = 0$. As a result, the exact range chosen to obtain the 'mid-rapidity' averages shown in Figs. 3 and 4 is not significant. Also, the distributions tend to get narrower for increasing centrality.

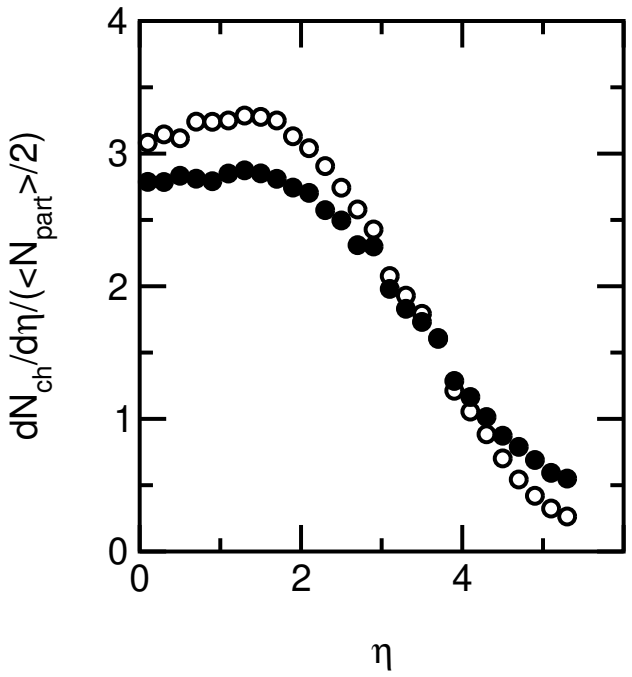

Fig. 6. This figure shows the same data as in the center left (filled circles; 35-45%) and bottom right (open circles; 0-6%) panels of Fig. 5 but now normalized to the number of participant pairs and superimposed.

In general, the shapes are not strongly dependent on centrality, although there are subtle differences which are illustrated in Fig. 6. In this figure, the center left (35-45%) and bottom right (0-6%) panels of Fig. 5 are shown as filled and open circles, respectively. In this case, the densities are once again normalized to the number of participant pairs. It is clear that most of the increase in normalized particle production shown in Fig. 4 for most central collisions occurs near mid-rapidity. One possibly surprising aspect of Fig. 6 is that particle production per participant actually rises with decreasing

centrality near beam and target rapidities (compare closed to open circles near $\eta \approx 5$). This results in a cross-over near $\eta \approx 3-4$ where the particle production per participant is essentially independent of centrality. The placement of the paddle trigger counters close to this rapidity region is therefore very fortuitous!

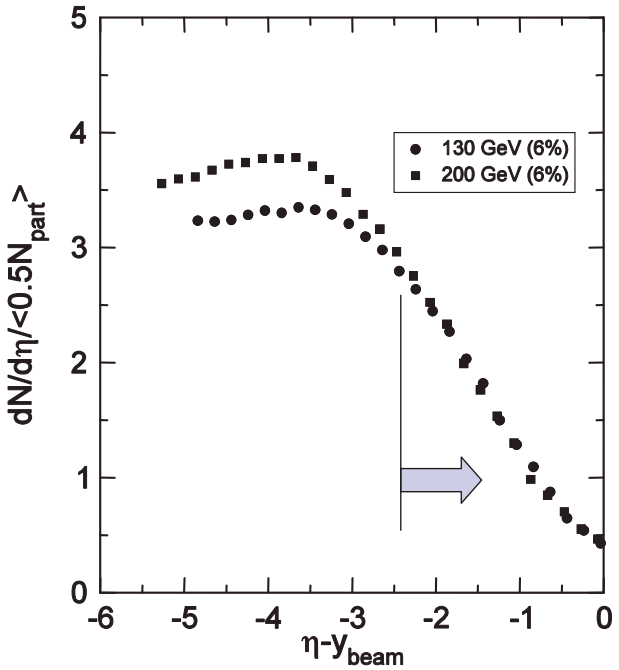

Fig. 7. This figure compares the charged particle pseudorapidity density normalized to the number of participant pairs for the most central 6% of the AuAu interactions at both 130 and 200 GeV. The horizontal axis has been shifted by the difference in the beam rapidity at the two energies.

Another interesting feature of the pseudorapidity distributions is the beam energy dependence of the region extending out to target or projectile rapidity. Fig. 7 shows normalized densities at 130 and 200 GeV. The 130 GeV data points are identical to those in Fig. 6 except that the horizontal axis has been shifted by the difference in beam rapidities between the two energies. As was seen for the centrality dependence, the dominant contribution to the rise in normalized particle production shown in Fig. 3 comes near mid-rapidity. In this case, the regions away from mid-rapidity, specifically within about 2.5 units of the target or projectile are indistinguishable between the two data sets. Very similar results were found for nucleon-nucleon collisions at energies ranging from 53 to 900 GeV[19] and

were attributed to fragmentation.

3.5. Multiplicity Summary

Phobos has made many significant contributions to the understanding of charged particle production at RHIC energies. These include extensive results on the energy, centrality, and rapidity dependence. In evaluating these results using any measure or model, it is clear that a system of very high density is being formed in the early stages of AuAu collisions. These data have already had an enormous impact on theoretical models including constraints on the initial conditions and subsequent evolution, as well as restricting the possible global properties and fundamental interactions (for example, hard versus soft processes). The near future will bring similar analyses of AuAu collisions at 20 GeV (run in November, 2001, specifically for Phobos) as well as a comparisons to 200 GeV (run in January, 2002). In addition, expanded analyses including more detailed studies, fluctuation, event shape, etc., are ongoing.

4. Spectrometer Results

The Phobos magnetic spectrometer was designed to track and identify particles near mid-rapidity. One primary focus of the design was the ability to extend these measurements to the lowest possible transverse momentum. However, with a reasonably large integrated magnetic field and Si detectors with small pixel sizes, the spectrometer also has good resolution for high $p_\perp$ studies. Particle identification for all tracks is provided by the average energy loss in the Si sensors. A typical sample is shown in Fig. 8. Detailed comparisons of expected and measured energy losses show that the resolution is about 7%.

Early analysis of identified particles focused on one of the most important open questions prior to the first RHIC data, namely the chemical environment of the system formed near mid-rapidity. Although many theorists expected that the net baryon density would smaller than seen in lower energy collisions, it was not clear what the value would be. There were even suggestions that exotic processes would lead to enhanced stopping at RHIC energies and therefore significant movement of baryon number away from the target and projectile rapidity [20].

The Phobos experiment has measured the ratios of yields of π^- to π^+, K^- to K^+ and antiprotons to protons near midrapidity (y from about 0.15 to about 0.8 for kaons and protons and about 0.3 to 1.4 for pions) [21]. The ratios were obtained by comparing the numbers of particles in events taken with opposite polarity so that the two charges were both bending in the same direction and thus had identical acceptances. The range of transverse

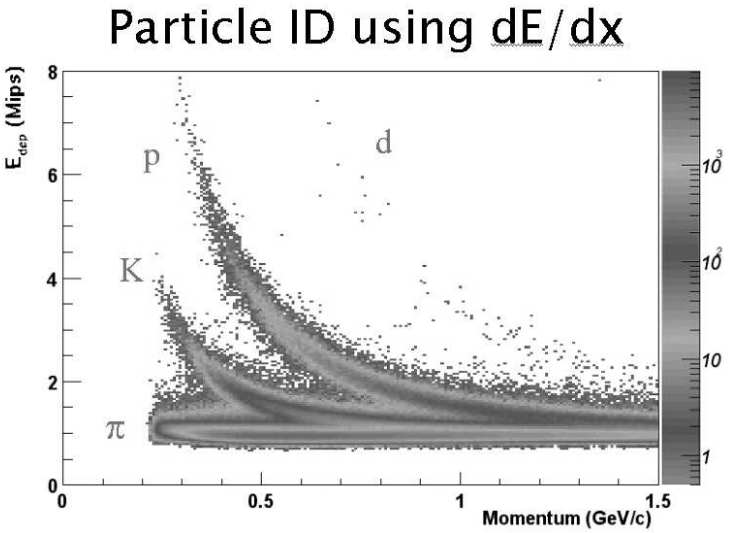

Fig. 8. Average energy loss in the spectrometer Si wafers is plotted versus the momentum of the track. Clear bands corresponding to the different particle types are seen.

momenta were about 50 to 500 MeV, 100 to 650 MeV and 150 to 900 MeV for pions, kaons, and protons, respectively. The ratios found for the most central 12% of AuAu collisions at 130 GeV were π^-/π^+=1.00±0.01±0.02, K^-/K^+=0.91±0.07±0.06, and $\overline{p}/p$=0.60±0.04±0.06, where the statistical uncertainty is listed followed by the systematic one. The deviation of the last ratio from 1.0 indicates that the system formed near mid-rapidity is not baryon-free. This observation can be made more quantitative by comparing to the predictions of a thermal model [22]. The results are shown in Fig. 9 where the particle ratios for kaons and protons have been calculated as a function of the baryon chemical potential. A freeze-out temperature of about 160-170 MeV was assumed, although the curves are not strongly dependent on this value. The horizontal bands show the allowed range given by the Phobos data. Note that the figure shows the kaon ratio as positive over negative charges. Both of the measured ratios are consistent with the range of chemical potential shown by the vertical band, 45±5 MeV. This is about a factor of 5-6 smaller than found for central collisions at SPS energies.

It remains for theoretical studies to determine the causes and implications of this measurement. Clearly, speculation about exotic large "stopping" at RHIC energies are ruled out. Nonetheless, it remains interesting

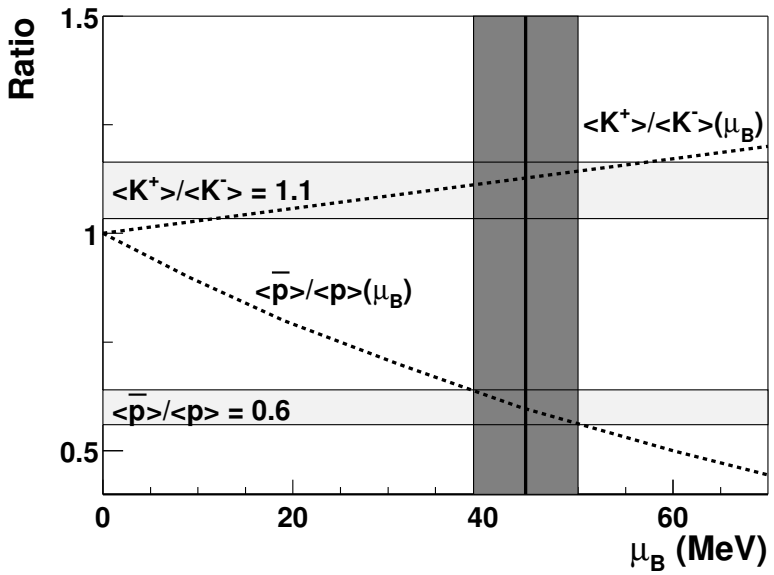

Fig. 9. This figure shows the predicted particles ratios for kaons and protons as a function of the baryon chemical potential. The horizontal bands correspond to the Phobos measured values. See text for discussion and references.

to explain how even this smaller remnant of the valence quark system has been transported over almost 6 units of rapidity.

Many additional analyses of spectrometer data are ongoing including similar ratios for 200 GeV AuAu collisions. In the near future, particle spectra (with and without particle identification), studies of low and high $p_\perp$ and HBT correlations will be available. For the farther future, additional analyses including resonances, studies versus centrality, rapidity, and reaction plane are being prepared.

5. The Low $p_\perp$ Future: Stopping Particles

In order to extend identified particle spectra to the lowest possible transverse momentum, the Phobos collaboration is analysing tracks which stop within the Si wafers of the spectrometer. By selecting only hits corresponding to large energy loss, the tracking becomes much easier. This is essential because low momentum tracks scatter significantly more than the average and so the various cuts for finding valid hit combinations need to be loosened considerably.

An example of early studies is shown in Fig. 10. The plots compare

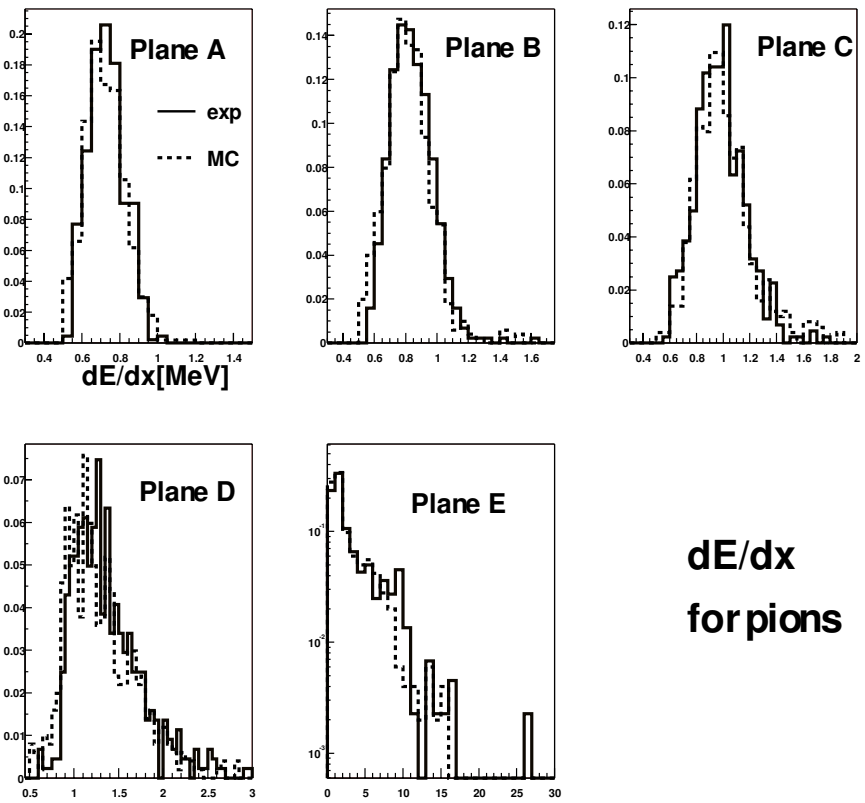

Fig. 10. This figure shows the predicted (dashed lines) and measured (solid lines) energy loss distributions in the first 5 Si layers of the spectrometer for pions that stop in the fifth layer. See text for discussion.

measured (solid lines) and predicted (dashed lines) energy loss distributions for pions which stop in the fifth layer of the spectrometer. The plots clearly show the steady increase in deposited energy as the pions slow down. The agreement for all layers is superb, indicating that a clean, well understood sample of pions is being extracted. Note the dramatically larger horizontal scale in the plot for Plane E (the last plane). Some fraction of the negative pions are captured onto the Si nuclei and fragment them. The detection of some of this fragmentation energy produces the long tail to higher energy loss. Thus, in this case, the particle yields can be partially separated into the two charge signs. Work is ongoing to understand the efficiency and

backgrounds for these stopping particles as well as extending the algorithms to particles stopping in other layers.

6. Conclusion

This talk has highlighted a few of the physics results obtained by the Phobos collaboration at RHIC. Many other, for example including flow [23], have not been discussed. The Phobos data have been critical in the early attempts to understand the conditions created in the new regime of heavy ion collisions at these high energies. The results have had a significant impact on the theoretical interpretation, including both global properties and fundamental interactions. More beam energies and beam species (including asymmetric systems such as pAu or dAu) are eagerly anticipated in future runs in order to continue the systematic study of varying initial conditions. For the farther future, various upgrades to the tracking, vertexing, and particle identification are being considered. The collaboration is looking forward to an exciting period of exploration in this new frontier.

REFERENCES

[1] B. B. Back *et al.*, *Nucl. Phys.* **A661**, 690 (1999).
[2] R. Nouicer *et al.*, *Nucl. Inst. Meth.* **A461**, 143 (2001).
[3] R. Bindel *et al.*, *Nucl. Inst. Meth.* **A474**, 38 (2001).
[4] J. M. Katzy *et al.*, *Nucl. Phys.* **A698**, 555c (2002).
[5] B. B. Back *et al.*, *Phys. Rev. Lett.* **85**, 3100 (2000).
[6] B. B. Back *et al.*, *Phys. Rev. Lett.* **88**, 22302 (2002).
[7] C. Adler *et al.*, *Phys. Rev. Lett.* **87**, 112303 (2001).
[8] F. Videbæk *et al.*, *Nucl. Phys.* **A698**, 29c (2002).
[9] K. Adcox *et al.*, *Phys. Rev. Lett.* **86**, 3500 (2001).
[10] L. Ahle *et al.*, *Phys. Lett. B* **476**, 1 (2000), L. Ahle *et al.*, *Phys. Lett. B* **490**, 53 (2000), B. B. Back *et al.*, *Phys. Rev. Lett.* **86**, 1970 (2001).
[11] J. Bächler *et al.*, *Nucl. Phys. A* **661**, 45 (1999).
[12] C. Blume *et al.*, *Nucl. Phys.* **A698**, 104c (2002).
[13] F. Abe *et al.*, *Phys. Rev. D* **41**, 2330 (1990).
[14] B. B. Back *et al.*, *Phys. Rev. C* **65**, 31901R (2002).
[15] B. B. Back *et al.*, nucl-ex/0201005, submitted to *Phys. Rev. C* (2002).
[16] D. Kharzeev and M. Nardi, *Phys. Lett. B* **507**, 121 (2001).
[17] D. Kharzeev and E. Levin, *Phys. Lett. B* **523**, 79 (2001).
[18] B. B. Back *et al.*, *Phys. Rev. Lett.* **87**, 102303 (2001).
[19] Alner *et al.*, *Z. Phys. C* **33**, 1 (1986).

[20] T. Schönfeld, *et al.*, *Mod. Phys. Lett.* **A8**, 2631 (1993).
[21] B. B. Back *et al.*, *Phys. Rev. Lett.* **87**, 102301 (2001).
[22] K. M. Redlich, *Nucl. Phys.* **A698**, 94c (2002).
[23] I. Park, *Nucl. Phys.* **A698**, 564c (2002).